Solar EUV-Enhancement and Thermospheric Disturbances

C. Briand, K. Doerksen, F. Deleflie

AGU ADVANCING EARTH AND SPACE SCIENCE

Space Weather®

RESEARCH ARTICLE
10.1029/2021SW002840

Solar EUV-Enhancement and Thermospheric Disturbances

C. Briand[1], K. Doerksen[2], and F. Deleflie[3]

[1]LESIA, Observatoire de Paris-PSL, CNRS, Sorbonne Université, Université de Paris, Meudon, France, [2]Planet Labs Inc., San Francisco, CA, USA, [3]IMCCE, Observatoire de Paris-PSL, CNRS, Sorbonne Université, Université de Lille, Paris, France

Key Points:

- One day solar EUV-enhancements induce thermospheric density perturbations that can form plateaus lasting half a day
- These density perturbations are large enough to be significant for satellite drag estimations
- These EUV-emissions can also be at the origin of weak D_{st} drops

Correspondence to:

C. Briand,
carine.briand@obspm.fr

Citation:

Briand, C., Doerksen, K., & Deleflie, F. (2021). Solar EUV-enhancement and thermospheric disturbances. *Space Weather*, *19*, e2021SW002840. https://doi.org/10.1029/2021SW002840

Received 11 JUL 2021
Accepted 15 NOV 2021

Author Contributions:

Conceptualization: C. Briand
Funding acquisition: C. Briand
Investigation: C. Briand, K. Doerksen, F. Deleflie
Methodology: C. Briand
Software: C. Briand, K. Doerksen
Validation: C. Briand
Writing – original draft: C. Briand
Writing – review & editing: K. Doerksen, F. Deleflie

Abstract The increase of energetic electromagnetic flux during solar flares and particle precipitation during geomagnetic activity are among the most important sources of neutral density disturbances to the Earth's thermosphere. However, disentangling the role of X and EUV radiation during solar flares is difficult due to the rarity of sufficiently isolated EUV-enhancements. Past work investigating the role of EUV-enhancements has been based on simulations only. This study focuses on the analysis of the response of the thermosphere to relatively long-lasting (between 1 and 2 days) EUV-enhancements. These events take place in isolation from coronal mass ejections, but often occur during the recovery phase of flare events. Using the Gravity Recovery and Climate Experiment and Challenging Minisatellite Payload accelerometer-derived density datasets, we show that the EUV-enhancements slow the thermosphere's recovery from a flare, and maintain a high level density perturbation "plateau" lasting several hours. The level of disturbance was found to be between 30% and 70% compared to the thermosphere's density without any disturbance. The duration of this plateau is long enough that it may be important for estimating satellite drag. Over the duration of the EUV-enhancements, Dst drops are also observed, indicating ring current activity. The proposed physical mechanism driving the Dst changes is linked to the increased production of O^+ ions of ionospheric origin, which may occur over the EUV-enhancement period.

Plain Language Summary Neutral density disturbances of the Earth's thermosphere are important from a satellite operation point of view, as short-term enhancements can cause increased drag effects to satellites in low Earth orbit, which can result, in the worst case, in necessary orbit mitigation for collision avoidance. The impact of X-solar radiation on the thermosphere has been studied extensively in the past, however there has been little to no work published specifically focusing on the EUV domain and its effects on the thermosphere's neutral density. Disentangling the role of X and EUV radiation is difficult due to the rarity of EUV-enhancements in isolation, and has been done in the past through simulations. This study focuses on EUV-enhancements lasting 1–2 days and occurring in absence from coronal mass ejection events. Often occurring after flares, we show that the main consequence of the EUV-enhancements is slowing the thermosphere's recovery to the density perturbation: a high level "density plateau" perturbation forms which lasts for several hours. Although rare, these kinds of event should be considered when estimating satellite drag, particularly with missions that require highly precise orbit ephemeris.

1. Introduction

Identifying all sources of disturbances to the neutral density of the Earth's thermosphere is of crucial interest for accurately estimating satellite drag on low Earth orbiting spacecraft and/or space debris for the computation of collision avoidance and mission planning (Berger et al., 2020; Vourlidas & Bruinsma, 2018). There is an increasingly critical need for real-time estimates of density variation (Gondelach & Linares, 2020). The thermospheric neutral density varies on a long-term scale (months to years), mostly driven by changes in the UV (120–200 nm) and EUV (10–120 nm, following the ISO21348 definition) irradiance (Guo et al., 2007). Coronal mass ejections (CMEs) and stream interaction regions (SIR) causing geomagnetic storms on Earth, and solar flares are the main drivers of density perturbations on a time-scale of hours to days (Emmert, 2015; Krauss et al., 2015; Qian & Solomon, 2012). If CMEs and flares are more frequent during maxima of the solar cycle, SIRs (and their periodic equivalent "co-rotating interaction region," CIR) are the main sources of disturbances during the solar cycle minimum (Burns et al., 2012; Chen et al., 2012, 2014).

Earth-crossing CMEs or SIRs can generate geomagnetic storms lasting for several days. During these periods, magnetospheric particle precipitations and Joule heating are the main sources of atmospheric heating. As a

consequence, the thermosphere expands, increasing the neutral density at high altitudes (≥500 km). The peak energy of CME-generated geomagnetic storms is higher than for CIR-generated storms, but the long duration of the Earth-crossing CIR implies that the total energy deposited during CIR can be larger than during a CME. Regarding the magnitude of density disturbance, a wide range of density disturbances have been reported: 20%–50% (Chen et al., 2012), 75% due to CIR (Lei et al., 2011), and up to 800% from severe CME-related storms (Bruinsma et al., 2006; Liu & Lühr, 2005). During daytime, the thermospheric density first increases at high latitudes in about 1 hr. Then, meridional circulation or traveling atmospheric disturbances (TADs) transport the energy toward lower latitudes in about 3–5 hr (Bruinsma et al., 2006; Oliveira et al., 2017; Sutton et al., 2009). The recovery phase after a geomagnetic storm is mostly controlled by the diffusion rate at the lowest altitudes (Richmond & Lu, 2000). Case studies have shown that the recovery time varies between about 1 day to more than 4 days (Bruinsma et al., 2006; Chen et al., 2012; Oliveira et al., 2017).

Solar flares produce an increase in X-ray irradiance of several orders of magnitude in a few minutes. In contrast to CME or SIR which take a few days to propagate from the Sun to the Earth, electromagnetic radiation needs only 8 min to reach the Earth's atmosphere. X-radiation increases excitation, ionization and dissociation of the atmospheric neutral components, down to the lowest D-layer. The excess energy from these absorption mechanisms is responsible for the heating of the thermosphere and density increase at high altitudes. The density increase at 400 km is approximately 10%–13% for X5-class flares (Le et al., 2012), and can reach up to 50% for strong flares (such as the X17 studied by Sutton et al. (2006)). Le et al. (2016) estimated from numerical modeling that density disturbances on the order of 200% from the quiet level could be reached at an altitude of 600 km from very strong X40-flares. These last two studies also show that the response of the thermosphere to flare forcing occurs between one to 4 hr, where stronger flares and higher altitudes result in faster response times, and the recovery time to return to quiet levels taking approximately 12 hr. Modeling by Pawlowski and Ridley (2008) have shown that this time is also controlled by the decay of the flare, the maximum of the density disturbance being reached almost at the end of the flare.

The cited papers have limited their analyses to X-ray flux variations, since their magnitude generally largely exceeds the EUV-flux, thus hiding the EUV's potential contribution to the density disturbance. However, EUV-flux dominates the ionization in the upper thermosphere, and induces neutral density perturbations (and temperature increases) above 400 km. Even in cases where the relative increase of EUV-flux is less than that of the X-radiation, density perturbations can reach more than 100% compared to its quiescent level (Huang et al., 2014). Additionally, flares occurring at the solar disk center appear to be more geo-effective than those arising closer from the limb. This effect is attributed to the contribution of the EUV-range, which is more optically thick compare to the X-domain and thus more absorbed on the limb than on the disk center (Donnelly, 1976; Le et al., 2011, 2012; Qian et al., 2010).

During flares, EUV-radiation is emitted from the chromospheric plasma heated by the electronic precipitation from the reconnection site. The hydrogen Lyman-α line (λ = 121.56 nm) dominates the long-wavelength part of the EUV spectrum. The short-wavelength part includes several lines of highly ionized species: HeII λ30.4 nm formed at 8.10^4 K at network cell boundaries, two iron lines (FeXV λ28.4 nm and FeXVI λ33.54 nm) formed at higher temperature (2.10^6 K), and CaXVIII line λ33.54 nm formed at temperatures above 5.10^6 K (Dere, 1978; Donnelly, 1976; Moses et al., 1997; Purcell & Widing, 1972), and signal non-thermal processes.

The aim of this study is to highlight and quantify the response of thermospheric neutral density to EUV-radiation forcing. We concentrate our analysis on four periods showing EUV-enhancements lasting one to 2 days, maximizing the potential for analysis of EUV-enhancements that exhibit strong forcing of the thermosphere, and isolated enough from other solar transients to disentangle their role from other sources of perturbation (as described in Section 2). To our knowledge, there has been no published work analyzing these kinds of events through observational data.

The remainder of the paper is structured as follows: in Section 2, the data and analysis procedures are explained. Section 3 presents the analysis of the selected events. Section 4 is dedicated to a discussion on the results before the conclusions presented on Section 5.

2. Data and Analysis Procedures

The EUV-fluxes were obtained from the Solar EUV Monitor (SEM) of SoHO (Judge et al., 1998). Compared to other instruments, SOHO/SEM presents the advantage of a continuous-time coverage for many years. The two channels 0.1–50 and 26–34 nm were used. The 26–34 nm channel efficiently signals temperature increase during solar flares and non-thermal processes in the active regions.

To optimize the chance of detecting neutral density perturbations due to EUV-enhancements, only events lasting at least 1 day were selected. The duration Δt was defined as the period when the EUV-flux remains above the defined, case-specific EUV quiet-level by more than 20%. The amplitude of the increase was not constrained, but only events with the same relative enhancement on the two channels of SoHO/SEM were kept. Indeed, during flares, we noticed that the 26–34 nm flux often increases much less than the 0.1–50 nm channel. This means that the short wavelengths (close to X-radiation) dominate the 0.1–50 nm range. Restricting our samples to events with an equivalent enhancement in the two channels has ensured that the EUV-range controls the brightening. These two criteria provide the best conditions for analyzing the EUV-flux's role in the disturbance of the atmosphere. To guarantee that the density disturbance results from EUV-forcing, we considered events as isolated as possible from other transients like interplanetary coronal mass ejections (ICMEs), and other geomagnetic activity. More precisely, the start-time of the EUV-enhancement event must be outside the period of an ICME, identified from the Richardson-Cane Near-Earth ICMEs list (Richardson & Cane, 2010). The interplanetary conditions (solar wind speed, magnetic field strength and orientation, mass flow and electron density) were also checked from OMNI database. To ensure a low level of geomagnetic activity, events were included in which the D_{st} remained above −50 nT (geomagnetic indices are obtained from the ISGI Webpage). Finally, EUV-enhancements are likely related to the presence of active regions, and it is therefore difficult to avoid the presence of flares during or before the time period of the EUV-increase. However, our analysis showed that the presence of flare events concurrent with EUV-enhancements actually helped to highlight the role of the EUV-flux to the perturbed thermosphere. Therefore, no criterion was applied regarding the presence of a flare in our analysis.

The thermospheric neutral density was derived from the highly sensitive accelerometers on-board the Gravity Recovery And Climate Experiment A and B (GRACE; Tapley et al., 2004), and the CHAllenging Minisatellite Payload (CHAMP; Reigber et al., 2002) satellites, which accurately measured the non-gravitational accelerations acting on the spacecraft orbiting the Earth at altitudes around 500 km for the former and 400 km for the latter. These measurements are free from any bias and drift due to the instruments, and, consequently any temporal variation is due to density perturbations acting on the spacecraft. The density data sets of CHAMP and GRACE provided by Mehta et al. (2017) were used, which cover the time period from 1 August 2002 until 31 December 2010.

The densities at a given time along a trajectory, $N(t)$, are expressed at a fixed altitude h_0, following the normalization procedure described in Bruinsma et al. (2006):

$$N(h_0, t) = N(h)\frac{N_M(h_0)}{N_M(z)} \tag{1}$$

with N being the observed density, N_M the density from a model, h the altitude, and h_0 the reference altitude. The normalization compensates for the density variations induced by the altitude variations of the spacecraft. Due to their large difference in altitude between the two spacecraft, h_0 differs: $h_0 = 480$ km for GRACE and 370 km for CHAMP. Usually, a thermospheric model is employed to obtain the density N_M. NRLMISE-00 (Picone et al., 2002) and DTM-2013 (Bruinsma, 2015) were tested, but their discrepancies with the observed density were much higher than the disturbance level we were looking for. An empirical density profile was built directly from the data for each event, averaging the density during quiet periods. The quiet periods encompassed several days before or after the event under study and excluded any geomagnetic disturbances. Throughout the remainder of the paper, the term “density” refers to “normalized density” and the term “neutral” will be omitted since only neutral density levels are concerned in this work.

The EUV-flux variations are strongly related to the presence of solar active regions. Thus, we cannot exclude that transients appear before the period of interest, and that EUV-brightenings start before the thermosphere recover its quiescent level. The density variation ΔN is then computed relative to a reference density level N_{ref}:

$$\Delta N(t) = \frac{N(t) - N_{ref}}{N_{ref}} \tag{2}$$

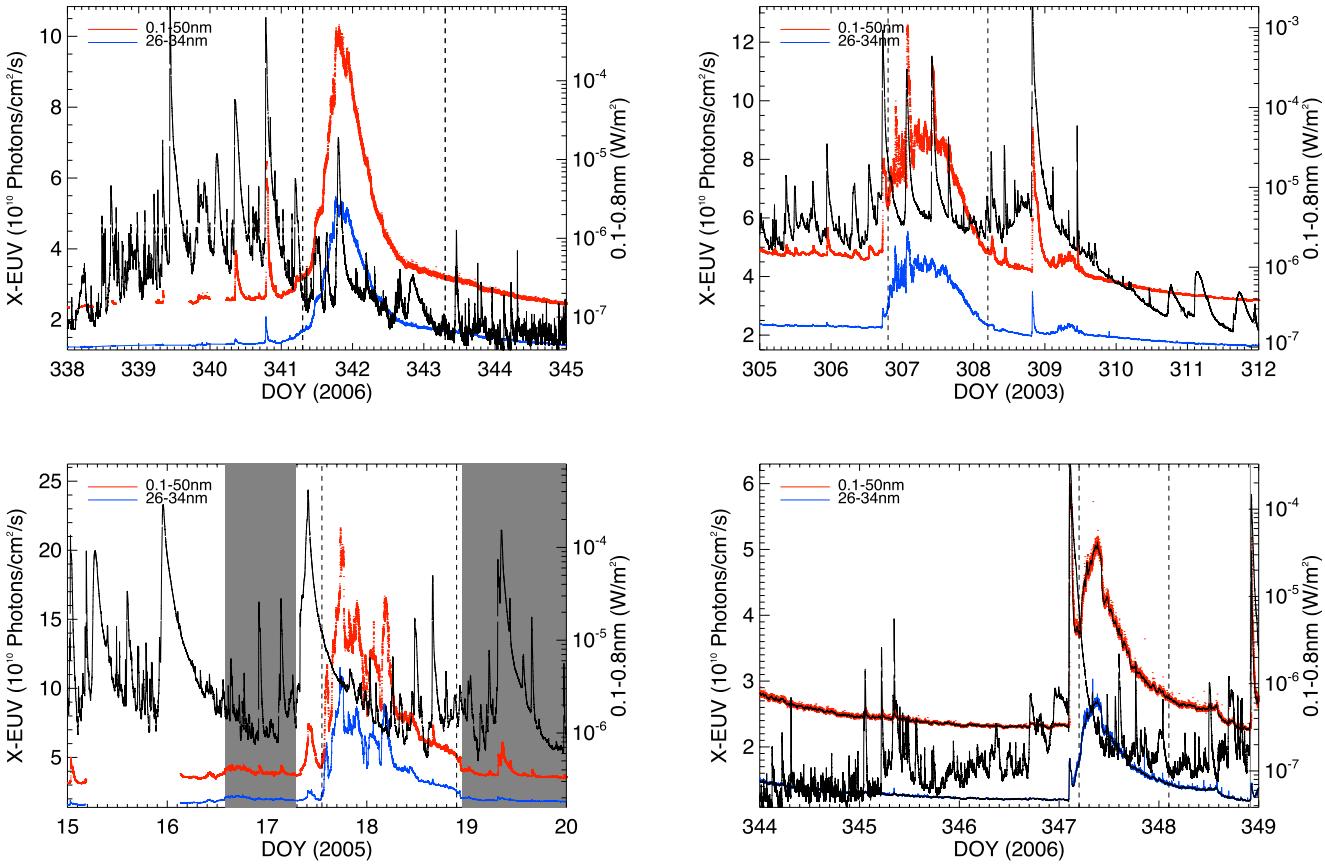

Figure 1. Time profile of the Solar EUV Monitor/X-EUV (red and blue, left ordinate-axis) and GOES/X-flux (black, right ordinate-axis) for the event of 4–10 December 2006 (top, left), November 2003 (top, right), January 2005 (bottom, left), and 10–15 December 2006 (bottom, right). The gray areas of the January 2005 event delineate the period of CME passages, as referenced by Richardson and Cane (2010). The vertical dashed lines indicate the interval Δt of the EUV-enhancement.

Therefore, N_{ref}, which is a priori different from the quiescent level used for the normalization (Equation 1), removes bias due to former forcing of the thermosphere. The procedure to deduce this reference level is specific to each event and will be detailed in each case.

3. Analysis

Large EUV-enhancements were infrequent events over the 8-year period of study (2002–2010), in particular in the 26–34 nm range. Only four events fulfilling the above conditions were found that enabled the analysis of the EUV-enhancements role to the thermospheric density perturbation from other solar activity. Figure 1 displays the two SEM EUV-channels together with the X-ray time profiles from GOES for those four events. The relevant characteristics for each selected period is summarized in Table 1. Following the usual terminology, an X*n* flare corresponds to $n.10^4$ W/m^2 flux in the 0.1–0.8 nm range of GOES satellite

3.1. First Event: 7 December 2006 (DOY341)

The longest EUV event of our sample started on 6 December 2006, peaked on 7 December, and returned to its quiet level on 8 December. The large active region (number 10930 on the NOAA catalog), located eastward of the central meridian (S06E31, that is 6° South from the solar equator and 31° East from the central meridian), was likely the origin of the electromagnetic activity. The time profile of the EUV and X radiation is shown on top left panel of Figure 1. The enhancement started after two X-class flares (X9.0 on 5 December and X6.5 on 6 December, respectively DOY339 and DOY340). Le et al. (2012) did not detect any disturbance from the X9.0 flare, attributing the lack of response to the Central Meridian Distance of the flare (S03E68). However, our density normalization procedure enables the detection of a weak density increase, initiated at high latitudes in the

Table 1
Characteristics of the EUV-Flux, Presented in Decreasing Order of Time Duration

	Δt	26–34 nm			0.1–50 nm		
Date	Days	Total energy	I_{max}	Background	Total energy	I_{max}	Background
7 December 2006	2.0	4.81	5.5	1.7	9.1	10	3.1
3 November 2003	1.5	4.78	4.4 (5.6)	2.3	9.8	8.7 (13)	4.8
17 January 2005	1.4	6.0	11	2.1	11	21	4.6
13 December 2006	1.0	1.5	3.0	1.2	2.9	6.0	2.4

Note. From left to right: date of peak flux; duration in days; total EUV energy (integral over Δt of the flux, for each range of wavelength) expressed in 10^{15}Photon/cm^2; peak magnitude of the flux value, in 10^{10}Photon/cm^2/s; irradiance background level prior to the enhancement, in 10^{10}Photon/cm^2/s. For the event of 2003, the peak value in parenthesis corresponds to the flare during the period while the other value corresponds to the average maximum – excluding the flare – during the whole period.

southern hemisphere followed by a propagation toward lower latitudes (Figure 2, top row). Unfortunately, the lack of EUV data during this X9.0 flare precludes an analysis of possible contributions from this wavelength range.

The period over which the EUV-enhancement occurred was relatively free from other types of forcing. Over the duration of the EUV-enhancement, only an M1.8 flare occurred, which was not expected to produce significant disturbances to the thermospheric density. In addition, the geomagnetic activity was low during the enhancement's development ($D_{st} > -50$ nT). Between 6 and 8 December, the two usual proxies for UV-flux were $F10.7 \approx 95$SFU and $F30 \approx 59$SFU.

The period of EUV-enhancement extended from DOY341 to DOY343. It is delimited by the black vertical dashed-lines on Figures 2 and 3. It occurred during the recovery phase of the X6.5-flare, which peaked 12 hr before the start of the EUV increase. The flare-source active region was very close to the solar central meridian (S06W23), which substantially impacted the thermosphere: a density peak occurred about 3 hr after the solar X-ray maximum (Figure 3). The X-flux had almost returned to its quiet level when the EUV-flux began to increase (Figure 1, top left). To quantify the impact of the EUV-flux only, the contribution on the density perturbation from the X6.5-flare had to be removed. Thus, the density recovery phase was evaluated with a decaying exponential, starting at the density peak (DOY340.9) and fitting the density in all latitudinal bins (shown with blue curves on Figure 3). The same decay rate τ_{decay} was applied to all bins, but was satellite dependent since their altitude was different. We have evaluated $\tau_{decay} = 1.5$ days for GRACE and $\tau_{decay} = 2.0$ days for CHAMP. This exponential function was used to evaluate the reference level N_{ref}, at the density peak-time, which enters in the computation of ΔN (Equation 2) (shown by crosses on Figure 3). It can be noted that in each latitudinal bin, the reference value was very close to the quiet level (displayed in green).

The bottom right panel of Figure 3 shows the maximum of ΔN versus latitude. The variations from one latitudinal bin to the other were not convincingly significant. Therefore, we defined δN as the average of $(\Delta N)_{max}$ over latitudes between $\pm 50°$, and its 1σ-standard deviation as uncertainty. CHAMP and GRACE were at almost the same Local Solar Time (LST, Table 2) during this event: 15:20 for GRACE and 16:30 for CHAMP. Both spacecraft detected a density increase in clear relation to the increase in the EUV flux, despite their altitude difference (at that time, GRACE orbit varied from 460 to 510 km while CHAMP orbit was confined between 350 and 380 km), with $\delta N = 0.71 \pm 0.07$ for GRACE and 0.61 ± 0.05 for CHAMP. Interestingly, the recovery time of the density was much longer than after the flare forcing, which can be attributed to the long duration of the intense EUV-flux.

A density ribbon is observed on DOY343 from the two spacecraft and is thus likely a real phenomenon. Its origin is still unknown. In their numerical study Pawlowski and Ridley (2011) described the possibility of a second perturbation "bump" caused by the development of TADs. This could explain the new bump observed 7 hr after the X6.5-flare first density-peak but probably not the bump of DOY343, which occurred 1 day after the EUV-related density-peak.

Despite the weak geomagnetic activity over the period of interest, a high-density level was observed at latitudes above 50° on both hemispheres (see Figure 2), that is unlikely related to the EUV-flux at these high latitudes. This point is further discussed in Section 4.

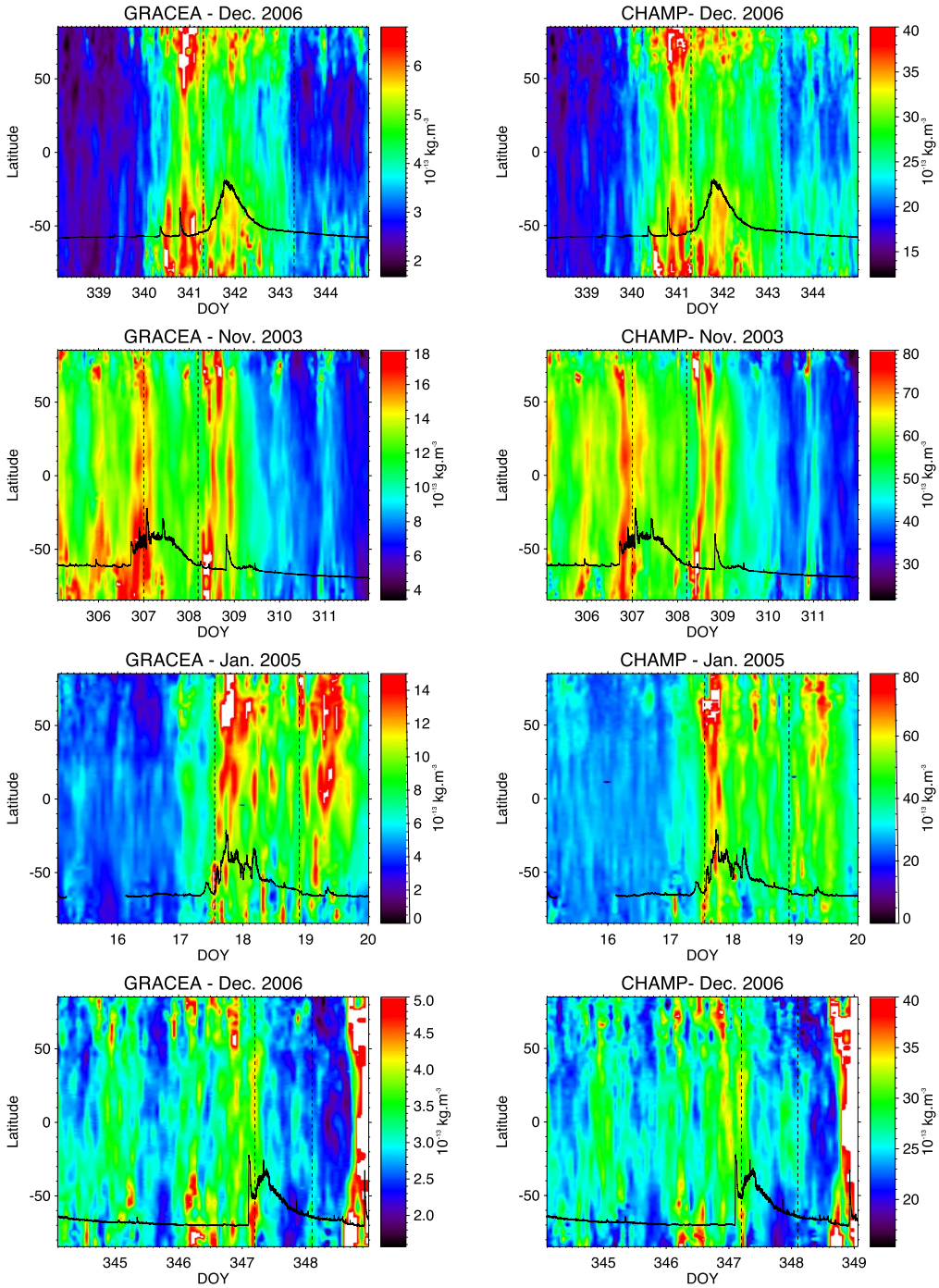

Figure 2. Daytime density map (color scale) w.r.t. latitude and time for the four periods studied, from top to bottom: 4–10 December 2006 (DOY338–DOY345), 1–6 November 2003 (DOY305–DOY312), 15–20 January 2005, and 10–15 December 2006 (DOY344–DOY349). Left column: GRACE-A (GRACE-B is similar) normalized at 480 km, and right column: Challenging Minisatellite Payload, normalized at 370 km. The vertical dashed lines delimit the time period of each EUV enhancement. The full black line displays the 26–34 nm solar flux on an arbitrary intensity scale. *Note the difference on density scale of the maps of the two spacecraft due to their difference of altitude normalization.*

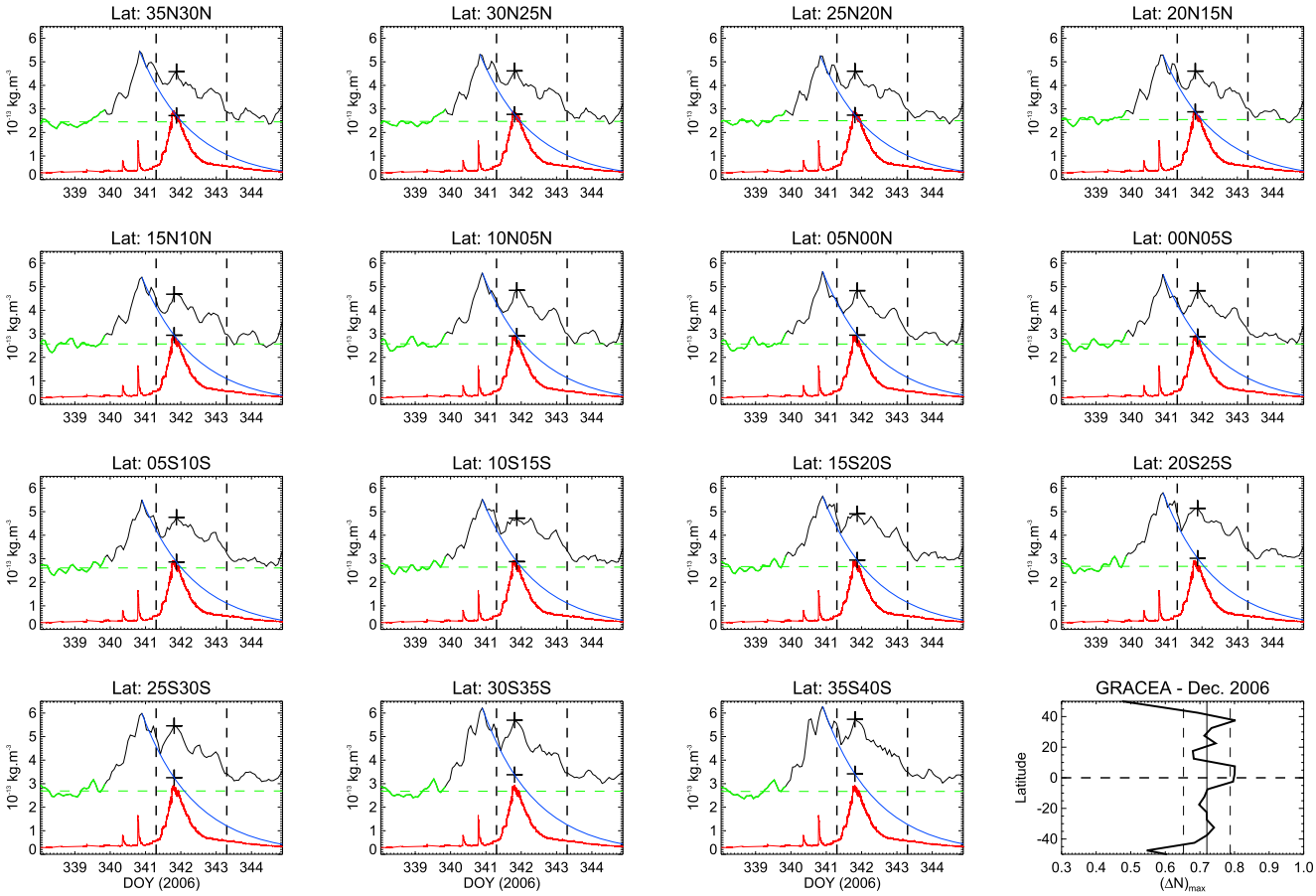

Figure 3. Density fluctuations inside latitudinal bins (limited on the graph to the latitudinal range ± 35°) for the first event of December 2006, and GRACE. The density curve highlighted in green shows the period selected to determine the quiet level (used for the data normalization), which level is finally indicated with the green-horizontal dashed-line. The decay fit (blue curve) mimics the recovery phase from the X6.5 flare. The red curve displays the EUV-flux on an arbitrary scale. The last bottom-right panel displays ΔN versus latitude. ΔN corresponds to the difference between the two crosses on each latitudinal bin: the upper cross is taken at the peak of the density curve, while the lower cross lays on the blue curve at the same time.

3.2. Second Event: 3 November 2003 (DOY307)

The period between 28 October to 5 November 2003 is known for its intense solar activity. Our second event of interest occurred during this period, beginning after a CME passing Earth and ending before an X17 flare. The EUV background increased at the end of an X8.3 flare (Figure 1, top right). The flare itself produced a weak signature in the 26–34 nm range. CHAMP and GRACE were separated by 3 hr in LST (15:40 for GRACE, 12:30

Table 2
Summary of the Density Disturbance

	δN		Local solar time	
Date	GRACE-A	CHAMP	GRACE-A	CHAMP
7 December 2006	0.71 ± 0.07	0.61 ± 0.05	15:20	16:30
11 November 2003	0.51 ± 0.07	0.39 ± 0.02	15:30	12:30
17 January 2005	0.62 ± 0.07	0.54 ± 0.05	18:35	08:00
13 December 2006	−0.09 ± 0.02	−0.025 ± 0.03	15:00	16:00

Note. The value is the average of $(\Delta N)_{max}$ over ±50° in latitude. The uncertainty correspond to the 1σ standard deviation over the same range of latitude. CHAMP, Challenging Minisatellite Payload; GRACE, Gravity Recovery and Climate Experiment A.

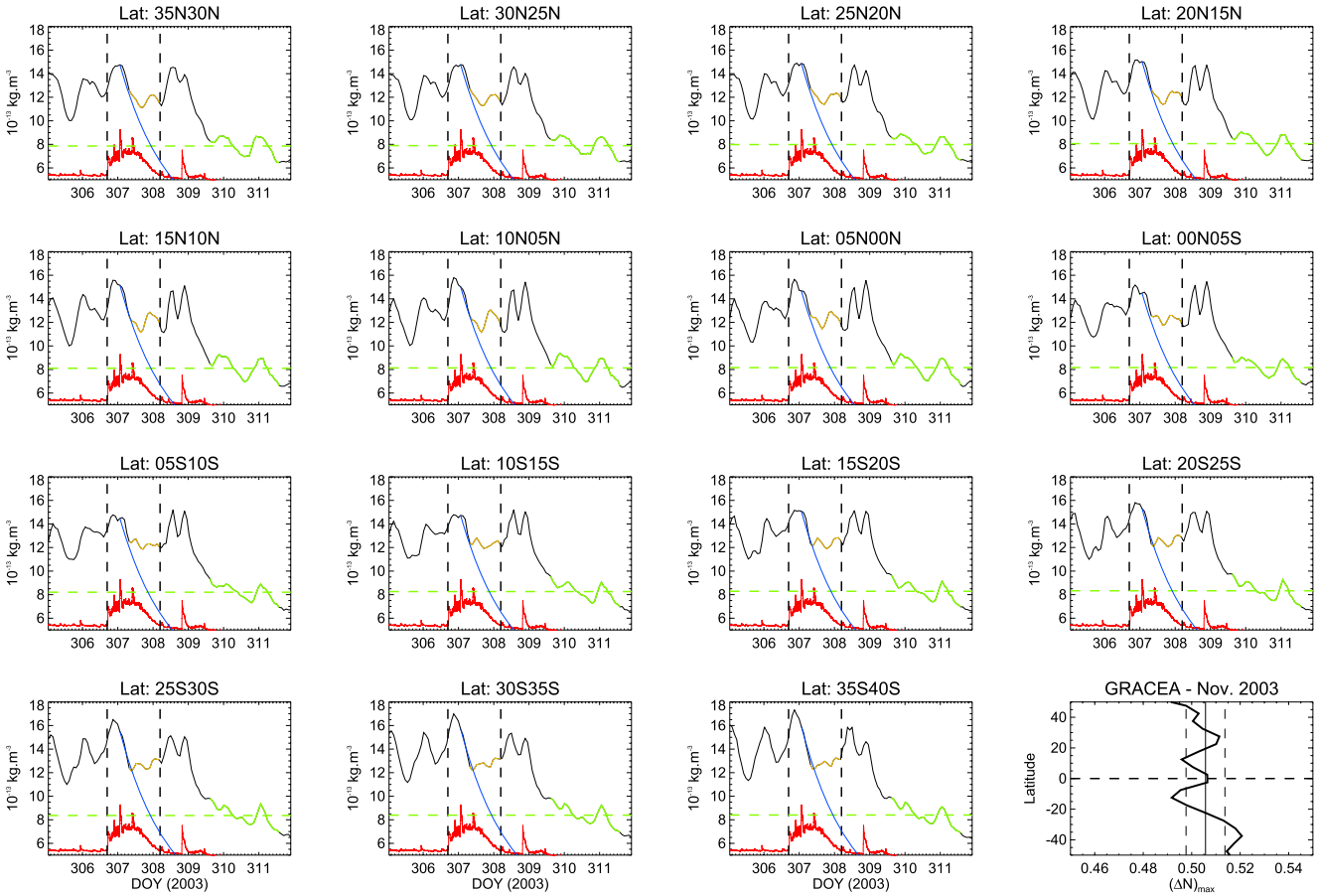

Figure 4. Density fluctuations inside latitudinal bins (limited on the graph to the latitudinal range ± 35°) for the event of November 2003, for Gravity Recovery and Climate Experiment. The green part of the density curve highlights the period used N_{quiet}, while the orange part shows the plateau period. The blue curve mimics the recovery phase after the flare, in absence of any other forcing. The last bottom-right panel displays ΔN versus latitude.

for CHAMP), yet both detected a density increase approximately 2.5 hr after the flare's peak (Figures 2 and 4). While the X-radiation was decreasing, the EUV continued to rise, and the density was in its recovery phase when a second X2.7 flare erupted. This flare showed a more pronounced increase in the two EUV ranges that augmented an already intense background density level. Despite its relative weakness, the X2.7 flare produced a noticeable density increase detected on the two spacecraft, with a time delay of about 2.5 hr. Finally, a third X3.9 flare occurred on DOY307, slightly after the EUV background level reached its maximum. The background level of the two EUV ranges was therefore still high, but the flare itself did not produce any significant increase in the 26–34 nm range, and showed only a weak increase in the other domain. This third flare may have produced a very weak density disturbance that can be detected on both satellite between latitude +5° and −10° (Figure 4). The density "plateau" observed after the end of the X3.9 in this event is particularly interesting. The plateau maintained a density greater than the quiet level despite the flare event and expected recovery phase ending, indicating that the source of this continued density forcing was the EUV radiation. As described in Section 3.1, to quantify the impact of the EUV radiation alone, the contribution of the second flare was removed. Its recovery phase was modeled with a decreasing exponential, with a single τ_{decay} for all the latitudinal bins and a given spacecraft. We estimated τ_{decay} = 1 day for GRACE and τ_{decay} = 1.4 days for CHAMP. Notably, the recovery phase of the DOY309 X17-flare was also accurately fitted with those values. We will discuss to this strong event at the end of this section. The period of the plateau (from DOY307.6 to DOY308.2) is highlighted in orange on Figure 4. As can be seen from this figure, the density of the recovery phase quickly reached the quiet level after the beginning of the plateau phase, thus we set $N_{ref} = N_{quiet}$ to evaluate ΔN (Equation 2). The average density during the plateau is used to evaluate ΔN. The bottom right panel of Figure 4 presents ΔN as a function of the latitudinal bins. The average density perturbation δN reached 0.50 ± 0.02 for GRACE and 0.39 ± 0.02 for CHAMP.

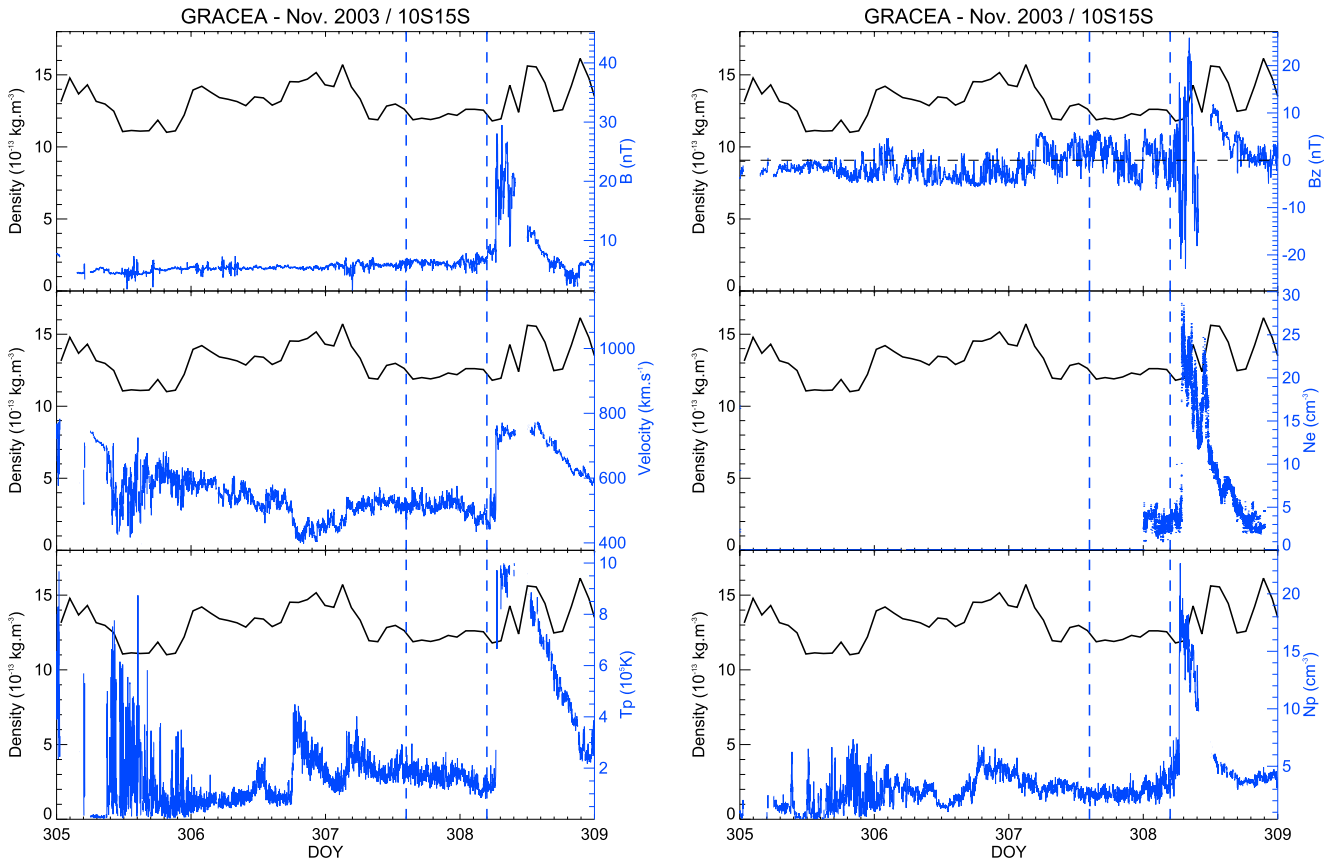

Figure 5. Solar wind parameters (blue curves) and density fluctuation of latitudinal bin 10S-15S versus DOY for the event of 2003. From top to bottom, left to right: the magnitude of the magnetic field, the B_z component of the magnetic field, the solar wind bulk velocity, the electron density, the proton temperature and the proton density. A shock is clearly observed after the second vertical dashed line, that is, the end of the EUV event.

To complete the description of this period, we discuss the analysis of the two density increases of DOY308. The first bump at DOY308.5 was due to a short-lasting shock (Figure 5), the second density perturbation at DOY308.9 was due to an X17 flare. Note however, that although it was much stronger than the X8.3 and X2.7 of DOY307, the density perturbation was not much greater. As can be checked from Figure 1, the increase in the two EUV ranges was very limited, which can explain the limited impact of this flare on the thermospheric density.

The main conclusion from this event is that the EUV time-evolution must also be taken into account in the assessment of density perturbation due to a flare, not only the X-component. The 1-day high-background level forcing induced a density increase of the same level as X-flare but for 12 hr, which may be long enough for a spacecraft to undergo an increased drag force that would affect its orbital position.

3.3. Third Event: 17 January 2005

The period between 15 and 20 January 2005 was also very active. Two CMEs passed the Earth (shown by the gray areas on Figure 1, bottom left) and three flares occurred: an X2.6 on 15 January, an X3.9 on 17 January, and an X1.3 on 19 January. Large fluxes of energetic particles arrived at the Earth on 20 January, producing ground level enhancement and modifications of the atmospheric components at very low altitudes (Jackman et al., 2011; Verronen et al., 2006). Between 17 and 19 January, F10.7 varied between 124 and 144SFU, while F30 varied between 76 and 82SFU. The geomagnetic activity remained low during the beginning of the EUV-event (Dst remained above −50 nT), but decreasing to −100 nT at the end of 18 January.

The first flare did not produce any density disturbance (see Figure 6) in spite of its central location (N15W05). Unfortunately, the analysis with the EUV-flux is impossible due to the lack of data during this period. The second flare was produced by the same active region, located more westward due to solar rotation (N15W25). The

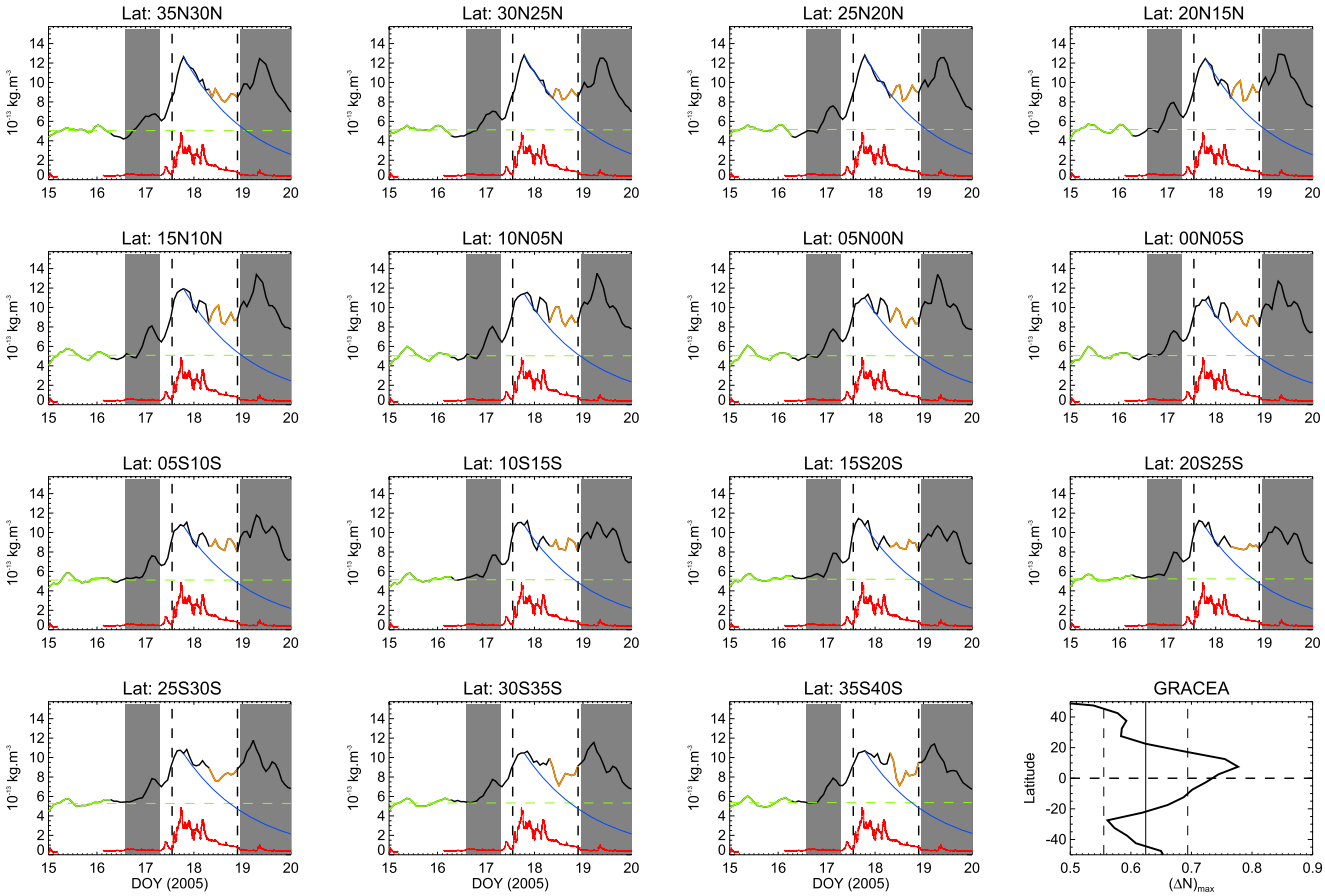

Figure 6. Density variation versus latitudes for the January 2005 and Gravity Recovery and Climate Experiment. The orange part of the density highlights the plateau period which serves for the evaluation of the density fluctuation attributed to the EUV-forcing. The gray areas symbolize periods of CME at Earth. The other color codes are equivalent as those of Figure 4.

increase in the two EUV-ranges was weak. Nonetheless, a density peak was observed 8 hr after the flare peak, which is an upper limit for a flare's impact as reported in the literature.

The EUV-enhancement duration was relatively short (1.4 days), but it showed the largest peak value and total energy of the four selected events of this study (Table 1). The enhancement started at 1300UT, during the decaying phase of the X3.8 flare. Thus, as performed for the previous events, the density disturbance due to the flare was removed by modeling the recovery phase with a decreasing exponential. For GRACE, the decay rate is $\tau_{decay} = 1.4$ days and 1 day for CHAMP. Figure 6 shows that the density did not return to the pre-event quiescent level throughout the period of EUV-enhancement. Instead, a high-level density plateau formed and remained for at least 12 hr. This plateau is thought to be the signature of the EUV-enhancement impact on the thermosphere. The fluctuations and the variation of the recovery phase with latitude render uncertain any estimate of the time limits of the plateau. However, since the two spacecraft observed this plateau almost simultaneously, we set its start-time at DOY18.3 and its end-time at the end of the EUV period (i.e., DOY18.9, before the second CME crossing). In contrast to the previous two events, the N_{ref} values may have been above the quiet level and change during the plateau period. Thus, N_{ref} was the value of the exponential function at the end of the plateau (or N_{Quiet} if it went below this value on given latitudinal bins).

The mean variation δN was 0.62 ± 0.07 for GRACE and 0.54 ± 0.05 for CHAMP. The decay model was not optimal for all latitudinal bins, which may change the δN by a few percent. Figure 7 displays the density variation versus latitudes for CHAMP. It is interesting to note that the details of the fluctuations during the plateau phase are almost identical for the two spacecraft (for example on bins 15N10N or 10N05N among others), which may

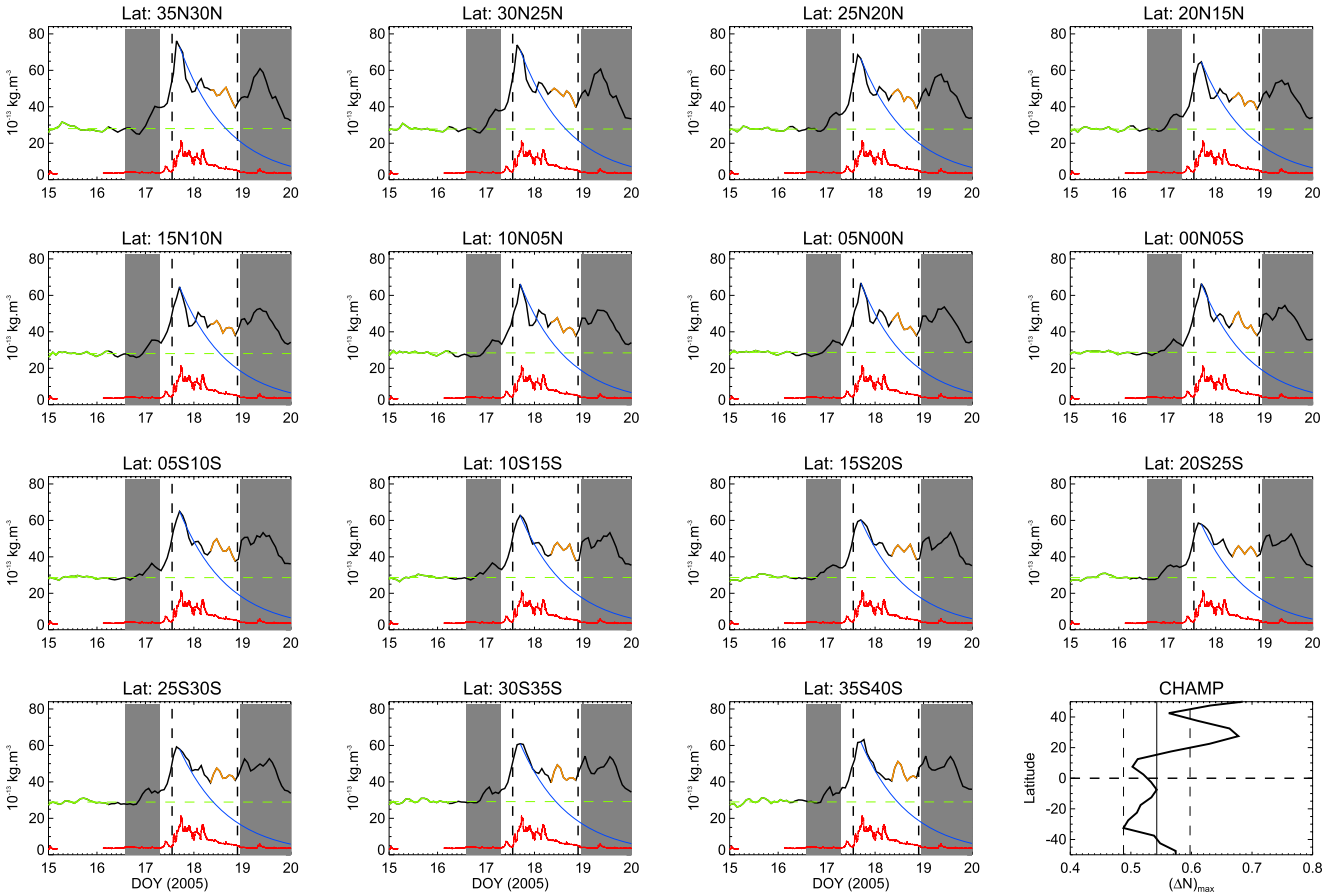

Figure 7. Same as Figure 6 for CHAMP.

indicate a real response of the thermosphere to the EUV-forcing. However, the peak of density in the southern hemisphere (35S40S) of CHAMP (about DOY308.4) is a trough of density on GRACE. These observations are interesting since the spacecraft were separated by about 100 km in altitude at that time, but almost opposite in LST; GRACE was on the dusk side (LST 18:35) while CHAMP was on the dawn side (LST 08:00), but a detailed analysis is beyond the scope of the present paper.

3.4. Fourth Event: 13 December 2006 (DOY347)

The fourth and final studied event occurred on 13 December 2006. Over the period, an X3.4-flare peaked at 0240UT on 13 December. The active region most likely at the origin of the EUV-flux enhancement was close to the solar central meridian (S06W23). The increase in the 26–34 nm range was weak during the flare, and the density fluctuations registered by both spacecraft were low (both close in LST – 15:00 for GRACE and 16:00 for CHAMP). The density maximum was reached about 2.5 hr after the flare peak. The EUV-flux decreased, before rising again, without flaring activity, and returned to its quiescent level after one day. As can be seen in Figure 8 the density recovery from the flare was rapid. As with the other events we have analyzed, the recovery phase was modeled by a decaying exponential. We find a recovery time of τ_{decay} = 0.5 days for GRACE and 0.7 days for CHAMP, twice as fast as the former events. Since the quiet level was reached very rapidly, we set $N_{ref} = N_{quiet}$ to evaluate the density due to the EUV-enhancement. For the two spacecraft, the density was even lower than the quiet level (Figure 8, bottom right panel), during the period DOY348-DOY349. This could be an example of thermospheric overcooling, as described by Zhang et al. (2019).

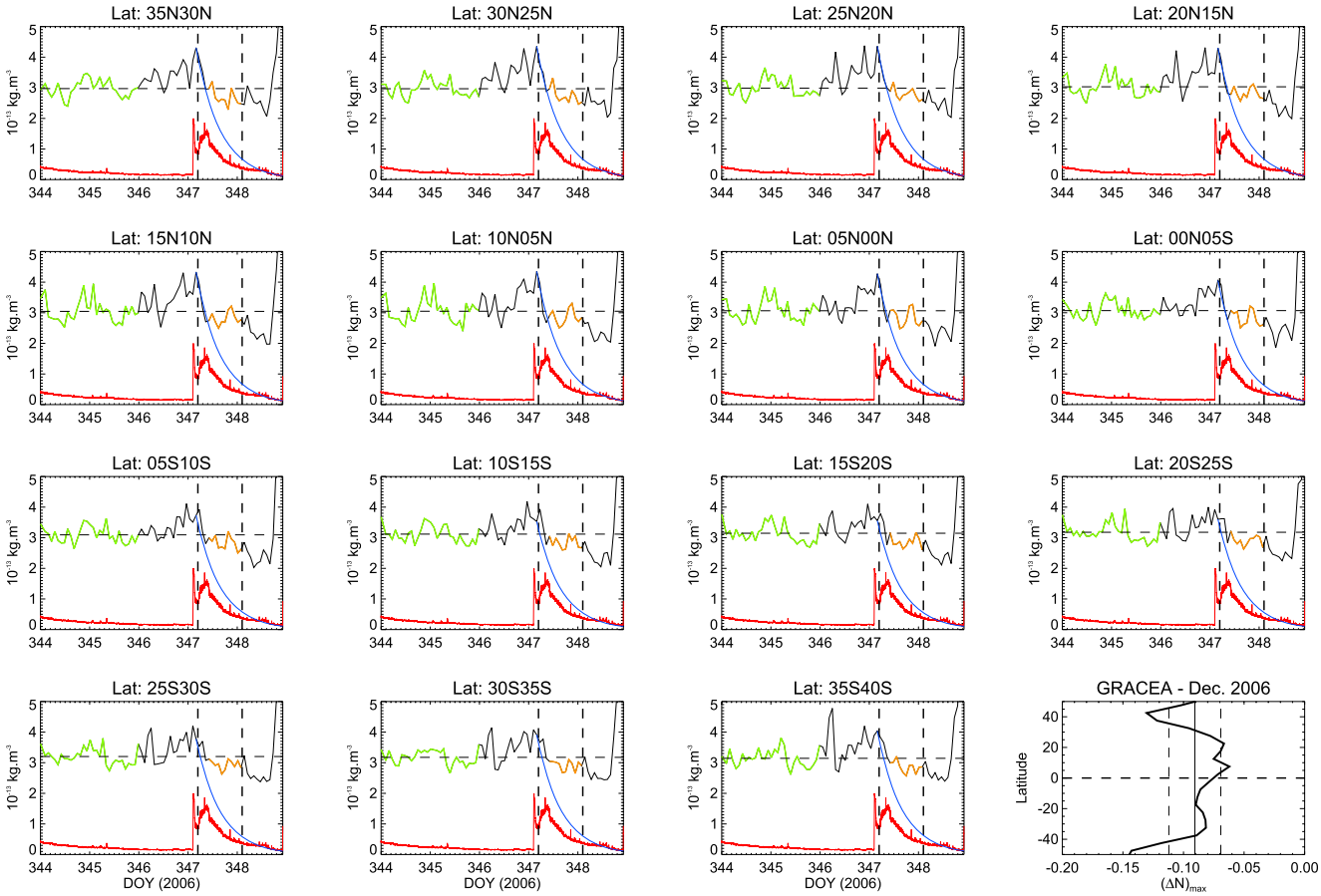

Figure 8. Density variation versus latitudes around 13 December 2006 and GRACE. The orange part of the density highlights the plateau period which serves for the evaluation of the density fluctuation attributed to the EUV-forcing. The other color codes are equivalent as those of Figure 4.

4. Discussion

The level of density perturbation produced and maintained by EUV-enhancements is comparable to that observed during flare events, and even larger solar activity. In contrast to flares, however the density recovery period is much longer. In three of the four cases, a well-defined density plateau formed, maintaining a high-density level for approximately half a day. Another consistent behavior of the events studied is the large latitudinal extension of the density perturbations. As noted by Liu et al. (2007), who studied the influence of X-rays on the thermosphere, the impact of the EUV-radiation can be felt at all latitudes, with an increase around equatorial regions. These longer duration and larger spatial extension perturbations are certainly important for treating satellite drag, but have been hitherto neglected in existing work.

The emission peak and the total energy deposited in the atmosphere are key parameters that control the density disturbances. Previous studies have shown that the density disturbances linearly increase in amplitude with the time-integrated energy and the peak amplitude in the 0.1–0.8 nm range (Le et al., 2015; Pawlowski & Ridley, 2011). In this context, we explored the potential relationship between EUV peak for one side and time-integrated energy on another side and δN. Since the EUV quiet-level also contributes to the atmosphere irradiation, it was included in the estimation of the peak magnitude and the integrated energy. Our results can also be compared with the ones of Le et al. (2012), which were obtained during flaring periods. Table 1 displays the energy integrated over the duration of each event ϵ and the maximum irradiance in the two EUV channels, while Table 2 summarizes the results of δN for the four events.

As expected, δN rises with the maximum peak intensity and the time-integrated energy (Figure 9). It seems to saturate for peak intensity above 5.10^{10} Photons/cm^2/s in the 26–34 nm range, and 10.10^{10} Photons/cm^2/s for the 0.1–50 nm range. The same saturation effect is observed for the energy, with limits of about 5.10^{15} Photons/cm^2

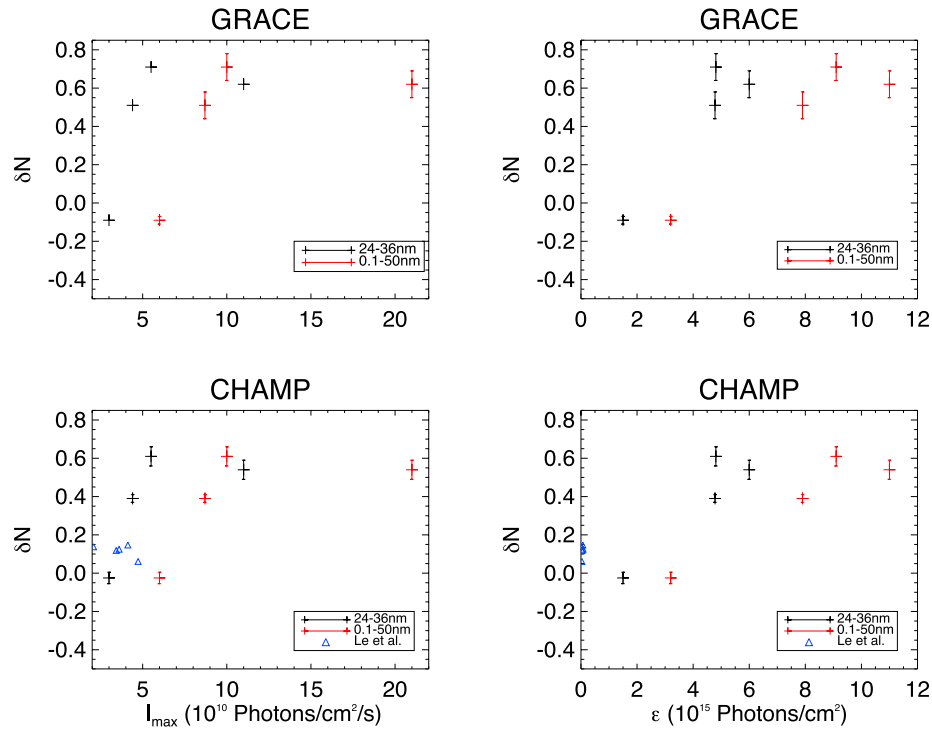

Figure 9. δN versus maximum peak intensity (left) and total energy ϵ (right) for the two spacecraft and the two ranges of wavelength. The blue triangles display the values obtained by Le et al. (2012).

in the 26–34 nm range and 9.10^{15} Photons/cm^2 in the 0.1–50 nm range. Due to the small number of events, the curves in Figure 9 cannot be considered as statistically significant. However, the results of Le et al. (2012) (obtained for the range 0.1–50 nm) are within the range of our values (blue diamonds on Figure 9). Also, although GRACE and CHAMP were treated independently, they present similar trends despite their orbital altitude differences. This makes us confident that the observed trend is real and highlights the need for further studies to identify new events.

The density disturbances are also observed at high latitudes (Figure 2), which is normally a signature of geomagnetic activity. However, the Dst for the selected periods showed only minor geomagnetic activity (the K_p index was also minor to moderate), except for a short period of a few hours when it reached almost −50 nT (Figure 10). To check if this weak activity originated from solar wind, the dawn-to-dusk electric field E_y and the dynamic pressure P_D were computed and compared to the evolution of Dst (Burton et al., 1975). E_y describes the injection rate of electrons into the ring current; a positive E_y induces a decrease of Dst. Conversely, the dynamic pressure P_D corresponds to a loss in the ring current; an increase of P_D produces to an increase of Dst. Figure 10 shows the time evolution Dst, E_y, and P_D for the four periods studied in this paper. In each case, P_D and E_y are almost constant during the variation period of the geomagnetic index, leading to the conclusion that the solar wind conditions are unlikely to have produced the Dst decrease.

During solar flares, EUV and X-radiation increase the ionization in the D and E layers, resulting in an increase of the ionospheric current systems, which in turn induces variations of the geomagnetic field. This is known as "Solar Flare Effects" (Curto, 2020; Tsurutani et al., 2009). During the periods of study, no convincing variation of the H-component of the magnetic field was observed by any ground-based magnetometers (from the SuperMAG network) simultaneously with the EUV-enhancements.

The increase of the number density of O^+ ions (and to a lesser extend a decrease of H^+) within the ring current is also known to produce immediate and short-duration Dst drops, even with reduced density fluctuations (Daglis, 1997). The large majority of O^+ ions are of ionospheric origin. We conjecture that large EUV-enhancements produce such ions on short time-scales as it does over longer timescales (Young et al., 1982), which in turn generate the observed Dst drops. However, we are not aware of O^+ density measurements for the periods considered

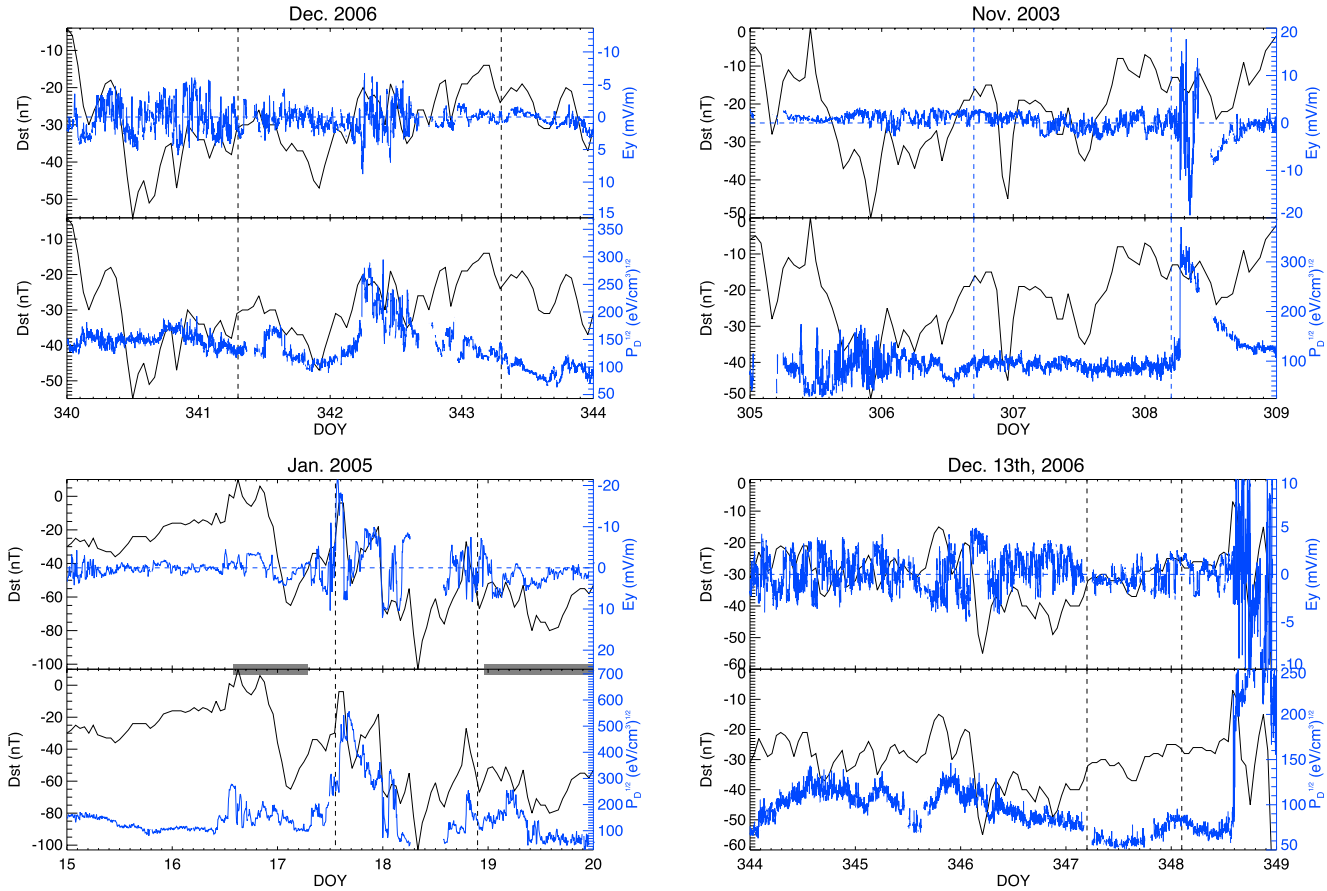

Figure 10. Dst geomagnetic index (in black) versus time compared to the E_y dawn-to-dusk electric field (top panel) and dynamic pressure (bottom panel), both in blue. *Note that the scale* of E_y is reversed for comparison with the paper of Burton et al. (1975). The time range is reduced compare to the previous graphs to focus on the periods of interest. The vertical dashed lines indicate the time interval Δt of the EUV-enhancement.

here with the time resolution necessary to check our hypothesis, and therefore suggest future work into this area of research to explore this theory.

5. Conclusions

Although the impact of solar X-radiation on the thermosphere has been intensively studied, in particular from observational analysis during major solar flares, little work has been reported concerning the EUV domain, except for long time variation events through simulations. On the short time-scale of a flare, disentangling the role of X- and EUV-enhancements is difficult, first because the X-range usually dominates the solar flux, and second because the two fluxes usually increase simultaneously. In this work, we have identified EUV-enhancements that clarify the role of X and EUV-radiation on the thermospheric density. The events are characterized by a long duration (above one day) and a clear enhancement in the two channels of SOHO/SEM, that is, in the 0.1–50 and 26–34 nm channels. The flux-rise in the 26–34 nm channel provides insight into the contribution of the EUV domain, since the 0.1–50 nm range includes a large contribution from X-ray. We studied the variation of the density at the altitudes of CHAMP and GRACE (400 km for the former, 500 km for the latter). Our study shows that the observed EUV-enhancements produce density increases that are large and long enough to be significant for models of spacecraft collision avoidance. It was found that, the density perturbation levels increased with the UV-emission maximum. No conclusion can be drawn regarding the impact of the time-integrated energy due to the reduce energy range explored by our data.

Dst variations indicate the activity of the ring current. O^+ ions are known to be at the origin of significant modification of the ring current during storms periods. We conjecture that large EUV increase can also be at the origin

of O^+ ions production. This aspect must still be confirmed by dedicated observations, and is an avenue of future work.

We focused our study on 1–2 days duration events as these were suspected to be the most favorable cases to generate density variations, which was confirmed. As a part of future work, it will be necessary to extend the survey to shorter duration events. The small number of events on which this analysis is based is not strongly statistically significant, but it displays trends in the data, especially in combination with other published work. A larger time period should be considered to increase the statistical significance, which will require access to larger databases of calibrated density measurements. The 1–2 days lasting events are infrequent, at least in isolation from CMEs, and require long and continuous time observational coverage to be detected.

Data Availability Statement

Neutral density data from: http://tinyurl.com/densitysets. CDAWEB: https://cdaweb.sci.gsfc.nasa.gov/index.html/. ISGI for the Dst values: http://isgi.unistra.fr/. CLS for the F10.7 and F30: https://spaceweather.cls.fr/services/radioflux/.

Acknowledgments
The authors thank the national institutes that support them. The authors also are grateful to the anonymous referees for their helpful comments.

References

Berger, T. E., Holzinger, M. J., Sutton, E. K., & Thayer, J. P. (2020). Flying through uncertainty. *Space Weather*, *18*(1), e02373. https://doi.org/10.1029/2019SW002373

Bruinsma, S. (2015). The DTM-2013 thermosphere model. *Journal of Space Weather and Space Climate*, *5*, A1. https://doi.org/10.1051/swsc/2015001

Bruinsma, S., Forbes, J. M., Nerem, R. S., & Zhang, X. (2006). Thermosphere density response to the 20-21 November 2003 solar and geomagnetic storm from CHAMP and GRACE accelerometer data. *Journal of Geophysical Research*, *111*(A6), A06303. https://doi.org/10.1029/2005JA011284

Burns, A. G., Solomon, S. C., Qian, L., Wang, W., Emery, B. A., Wiltberger, M., & Weimer, D. R. (2012). The effects of corotating interaction region/high speed stream storms on the thermosphere and ionosphere during the last solar minimum. *Journal of Atmospheric and Solar-Terrestrial Physics*, *83*, 79–87. https://doi.org/10.1016/j.jastp.2012.02.006

Burton, R. K., McPherron, R. L., & Russell, C. T. (1975). An empirical relationship between interplanetary conditions and Dst. *Journal of Geophysical Research*, *80*(31), 4204–4214. https://doi.org/10.1029/JA080i031p04204

Chen, G.-M., Xu, J., Wang, W., & Burns, A. G. (2014). A comparison of the effects of CIR- and CME-induced geomagnetic activity on thermospheric densities and spacecraft orbits: Statistical studies. *Journal of Geophysical Research*, *119*(9), 7928–7939. https://doi.org/10.1002/2014JA019831

Chen, G.-M., Xu, J., Wang, W., Lei, J., & Burns, A. G. (2012). A comparison of the effects of CIR- and CME-induced geomagnetic activity on thermospheric densities and spacecraft orbits: Case studies. *Journal of Geophysical Research*, *117*(A8), A08315. https://doi.org/10.1029/2012JA017782

Curto, J. J. (2020). Geomagnetic solar flare effects: A review. *Journal of Space Weather and Space Climate*, *10*, 27. https://doi.org/10.1051/swsc/2020027

Daglis, I. A. (1997). The role of magnetosphere-ionosphere coupling in magnetic storm dynamics. In *Magnetic storms* (pp. 107–116). American Geophysical Union (AGU). Retrieved from https://agupubs.onlinelibrary.wiley.com

Dere, K. P. (1978). Spectral lines observed in solar flares between 171 and 630 Angstroms. *The Astrophysical Journal*, *221*, 1062–1067. https://doi.org/10.1086/156110

Donnelly, R. F. (1976). Empirical models of solar flare X ray and EUV emission for use in studying their E and F region effects. *Journal of Geophysical Research*, *81*(25), 4745–4753. https://doi.org/10.1029/JA081i025p04745

Emmert, J. T. (2015). Thermospheric mass density: A review. *Advances in Space Research*, *56*(5), 773–824. https://doi.org/10.1016/j.asr.2015.05.038

Gondelach, D. J., & Linares, R. (2020). Real-time thermospheric density estimation via two-line element data assimilation. *Space Weather*, *18*(2), e02356. https://doi.org/10.1029/2019SW002356

Guo, J., Wan, W., Forbes, J. M., Sutton, E., Nerem, R. S., Woods, T. N., et al. (2007). Effects of solar variability on thermosphere density from CHAMP accelerometer data. *Journal of Geophysical Research*, *112*(A10), A10308. https://doi.org/10.1029/2007JA012409

Huang, Y., Richmond, A. D., Deng, Y., Chamberlin, P. C., Qian, L., Solomon, S. C., et al. (2014). Wavelength dependence of solar irradiance enhancement during X-class flares and its influence on the upper atmosphere. *Journal of Atmospheric and Solar-Terrestrial Physics*, *115*, 87–94. https://doi.org/10.1016/j.jastp.2013.10.011

Jackman, C. H., Marsh, D. R., Vitt, F. M., Roble, R. G., Randall, C. E., Bernath, P. F., et al. (2011). Northern Hemisphere atmospheric influence of the solar proton events and ground level enhancement in January 2005. *Atmospheric Chemistry and Physics*, *11*(13), 6153–6166. https://doi.org/10.5194/acp-11-6153-2011

Judge, D. L., McMullin, D. R., Ogawa, H. S., Hovestadt, D., Klecker, B., Hilchenbach, M., et al. (1998). First Solar EUV Irradiances Obtained from SOHO by the CELIAS/SEM. *Solar Physics*, *177*, 161–173. https://doi.org/10.1023/A:1004929011427

Krauss, S., Temmer, M., Veronig, A., Baur, O., & Lammer, H. (2015). Thermospheric and geomagnetic responses to interplanetary coronal mass ejections observed by ACE and GRACE: Statistical results. *Journal of Geophysical Research: Space Physics*, *120*(10), 8848–8860. https://doi.org/10.1002/2015JA021702

Le, H., Liu, L., He, H., & Wan, W. (2011). Statistical analysis of solar EUV and X-ray flux enhancements induced by solar flares and its implication to upper atmosphere. *Journal of Geophysical Research*, *116*(A11), A11301. https://doi.org/10.1029/2011JA016704

Le, H., Liu, L., Ren, Z., Chen, Y., Zhang, H., & Wan, W. (2016). A modeling study of global ionospheric and thermospheric responses to extreme solar flare. *Journal of Geophysical Research: Space Physics*, *121*(1), 832–840. https://doi.org/10.1002/2015JA021930

Le, H., Liu, L., & Wan, W. (2012). An analysis of thermospheric density response to solar flares during 2001–2006. *Journal of Geophysical Research*, *117*(3), 4–11. https://doi.org/10.1029/2011JA017214

Le, H., Ren, Z., Liu, L., Chen, Y., & Zhang, H. (2015). Global thermospheric disturbances induced by a solar flare: A modeling study. *Earth Planets and Space*, *67*, 3. https://doi.org/10.1186/s40623-014-0166-y

Lei, J., Thayer, J. P., Wang, W., & McPherron, R. L. (2011). Impact of CIR storms on thermosphere density variability during the solar minimum of 2008. *Solar Physics*, *274*(1–2), 427–437. https://doi.org/10.1007/s11207-010-9563-y

Liu, H., & Lühr, H. (2005). Strong disturbance of the upper thermospheric density due to magnetic storms: CHAMP observations. *Journal of Geophysical Research*, *110*(A9), A09S29. https://doi.org/10.1029/2004JA010908

Liu, H., Lühr, H., Watanabe, S., KöHler, W., & Manoj, C. (2007). Contrasting behavior of the thermosphere and ionosphere in response to the 28 October 2003 solar flare. *Journal of Geophysical Research*, *112*(A7), A07305. https://doi.org/10.1029/2007JA012313

Mehta, P. M., Walker, A. C., Sutton, E. K., & Godinez, H. C. (2017). New density estimates derived using accelerometers on board the CHAMP and GRACE satellites. *Space Weather*, *15*, 558–576. https://doi.org/10.1002/2016SW001562

Moses, D., Clette, F., Delaboudinière, J. P., Artzner, G. E., Bougnet, M., Brunaud, J., et al. (1997). EIT observations of the extreme ultraviolet sun. *Solar Physics*, *175*(2), 571–599. https://doi.org/10.1023/A:1004902913117

Oliveira, D. M., Zesta, E., Schuck, P. W., & Sutton, E. K. (2017). Thermosphere global time response to geomagnetic storms caused by coronal mass ejections. *Journal of Geophysical Research: Space Physics*, *122*(10), 10762–10782. https://doi.org/10.1002/2017JA024006

Pawlowski, D. J., & Ridley, A. J. (2008). Modeling the thermospheric response to solar flares. *Journal of Geophysical Research*, *113*, A10309. https://doi.org/10.1029/2008JA013182

Pawlowski, D. J., & Ridley, A. J. (2011). The effects of different solar flare characteristics on the global thermosphere. *Journal of Atmospheric and Solar-Terrestrial Physics*, *73*(13), 1840–1848. https://doi.org/10.1016/j.jastp.2011.04.004

Picone, J. M., Hedin, A. E., Drob, D. P., & Aikin, A. C. (2002). NRLMSISE-00 empirical model of the atmosphere: Statistical comparisons and scientific issues. *Journal of Geophysical Research*, *107*(A12), 1468. https://doi.org/10.1029/2002JA009430

Purcell, J. D., & Widing, K. G. (1972). Rocket observation of Ar XII-XVI Ca XIV-XVIII and Fe XIV, XV, XXIV in the extreme-ultraviolet spectrum of a solar flare. *The Astrophysical Journal*, *176*, 239. https://doi.org/10.1086/151626

Qian, L., Burns, A. G., Chamberlin, P. C., & Solomon, S. C. (2010). Flare location on the solar disk: Modeling the thermosphere and ionosphere response. *Journal of Geophysical Research*, *115*(A9), A09311. https://doi.org/10.1029/2009JA015225

Qian, L., & Solomon, S. C. (2012). Thermospheric density: An overview of temporal and spatial variations. *Space Science Reviews*, *168*(1–4), 147–173. https://doi.org/10.1007/s11214-011-9810-z

Reigber, C., Lühr, H., & Schwintzer, P. (2002). CHAMP mission status. *Advances in Space Research*, *30*(2), 129–134. https://doi.org/10.1016/S0273-1177(02)00276-4

Richardson, I. G., & Cane, H. V. (2010). Near-Earth interplanetary coronal mass ejections during solar cycle 23 (1996–2009): Catalog and summary of properties. *Solar Physics*, *264*, 189–237. https://doi.org/10.1007/s11207-010-9568-6

Richmond, A. D., & Lu, G. (2000). Upper-atmospheric effects of magnetic storms: A brief tutorial. *Journal of Atmospheric and Solar-Terrestrial Physics*, *62*(12), 1115–1127. https://doi.org/10.1016/S1364-6826(00)00094-8

Sutton, E. K., Forbes, J. M., & Knipp, D. J. (2009). Rapid response of the thermosphere to variations in Joule heating. *Journal of Geophysical Research*, *114*(A4), A04319. https://doi.org/10.1029/2008JA013667

Sutton, E. K., Forbes, J. M., Nerem, R. S., & Woods, T. N. (2006). Neutral density response to the solar flares of October and November, 2003. *Geophysical Research Letters*, *33*(22), 1–5. https://doi.org/10.1029/2006GL027737

Tapley, B. D., Bettadpur, S., Watkins, M., & Reigber, C. (2004). The gravity recovery and climate experiment: Mission overview and early results. *Geopysical Research Letters*, *31*(9), L09607. https://doi.org/10.1029/2004GL019920

Tsurutani, B. T., Verkhoglyadova, O. P., Mannucci, A. J., Lakhina, G. S., Li, G., & Zank, G. P. (2009). A brief review of "solar flare effects" on the ionosphere. *Radio Science*, *44*(A5), RS0A17. https://doi.org/10.1029/2008RS004029

Verronen, P. T., Seppälä, A., Kyrölä, E., Tamminen, J., Pickett, H. M., & Turunen, E. (2006). Production of odd hydrogen in the mesosphere during the January 2005 solar proton event. *Geophysical Research Letters*, *33*(24), L24811. https://doi.org/10.1029/2006GL028115

Vourlidas, A., & Bruinsma, S. (2018). EUV irradiance inputs to thermospheric density models: Open issues and path forward. *Space Weather*, *16*(1), 5–15. https://doi.org/10.1002/2017SW001725

Young, D. T., Balsiger, H., & Geiss, J. (1982). Correlations of magnetospheric ion composition with geomagnetic and solar activity. *Journal of Geophysical Research*, *87*(A11), 9077–9096. https://doi.org/10.1029/JA087iA11p09077

Zhang, Y., Paxton, L. J., Lu, G., & Yee, S. (2019). Impact of nitric oxide, solar EUV and particle precipitation on thermospheric density decrease. *Journal of Atmospheric and Solar-Terrestrial Physics*, *182*, 147–154. https://doi.org/10.1016/j.jastp.2018.11.016